Contents lists available at ScienceDirect

# Journal of King Saud University – Engineering Sciences

journal homepage: www.sciencedirect.com

Original article

# A dependence study: Molecular weight of polyethylene glycol (PEG) ON La$_{0.7}$Sr$_{0.3}$Co$_{0.2}$Fe$_{0.8}$O$_{3-\delta}$ (LSCF 7328) hollow fiber membrane for oxygen permeation

Hamzah Fansuri [a,*], Alfia Dewi Masyitoh [a], Silvana Dwi Nurherdiana [a], Wahyu Prasetyo Utomo [a], Triyanda Gunawan [a], Nurul Widiastuti [a], Mohd Hafiz Dzarfan Othman [b], Ahmad Fauzi Ismail [b], Subaer [c]

[a] Department of Chemistry, Faculty of Science and Data Analytics, Institut Teknologi Sepuluh Nopember (ITS), Kampus ITS Sukolilo, Surabaya 60111, Indonesia
[b] Advanced Membrane Technology Research Centre (AMTEC), School of Chemical and Energy Engineering, Universiti Teknologi Malaysia (UTM), Johor Bahru 81310, Malaysia
[c] Material Physics Laboratory, Physics Department, Universitas Negeri Makassar, Jalan Mallengkeri, Parang Tambung, Makassar 90224, Indonesia

ARTICLE INFO

ABSTRACT

In an effort to further improvement of LSCF hollow fiber membrane properties in oxygen purification applications, this work studied the use of polyethylene glycol (PEG) with a different molecular weights of 2000, 3400 and 6000 Da as a pore former. A well-prepared hollow fiber membrane was successfully fabricated via extrusion followed by a sintering method. The results showed that the addition of PEG increased the viscosity of the dope suspension and formed a constant asymmetric pore configuration of the membrane after sintering at 1250 °C. The increasing molecular weight of PEG also leads to a decrease in the mechanical strength of the membranes, indicating that finger-like pores were sacrificed by forming irregular pores. The gas tightness was also examined under room temperature which showed that membrane with PEG 3400 achieved the best tightness with the nitrogen permeability of $3.55 \times 10^{-5}$ mol·m$^{-2}$·s$^{-1}$·Pa$^{-1}$. The oxygen permeation of the membranes was also influenced by the addition of PEG, where the highest oxygen permeation flux of $6.07 \times 10^{-8}$ mol·cm$^{-2}$·s$^{-1}$ was obtained using a hollow fiber membrane with PEG 3400 due to the existence of the lowest dense layer thickness.

© 2021 The Authors. Production and hosting by Elsevier B.V. on behalf of King Saud University. This is an open access article under the CC BY-NC-ND license (http://creativecommons.org/licenses/by-nc-nd/4.0/).

## 1. Introduction

Perovskite oxide-based mixed ionic-electronic conductor (MIEC) such as LSCF in a membrane form has been extensively studied in recent decades (Sajidah et al., 2018). The membranes show their ability to deliver oxygen ions from the air through the perovskite crystal lattice (Wang et al., 2017). Based on this capability, it shows higher potential to be used in oxygen controlled catalytic processes such as partial oxidation of methane reaction and solid oxide fuel cell application (Ettouney et al., 1995).

The unique mechanism of oxygen transfer in MIEC membrane also offer alternative ways for oxygen separation and purification

from the air. Proven and mature oxygen separation technology, namely cryogenic distillation and pressure swing adsorption. The cryogenic distillation needs very low temperature while pressure swing adsorption has a problem on abrasion of adsorbent (mostly zeolite) due to pressure swing process (Akulinin et al., 2020). In the last decade, researchers develop membrane for oxygen separation by utilizing zeolitic materials and carbon molecular sieves. However, they exhibit an insufficient performance to separate oxygen from the air because the separation depends on the pore size (Murali et al., 2013; Rossetti et al., 2016) while the size of gasses are similar.

In addition to its constituent materials, the pore configuration of the membrane also plays an important role in determining the MIEC membrane performance. Flat membranes, in the form of pellets (disc), are widely used in various studies. However, the surface area of flat membrane is small that make them less suitable for large scale application. The thickness directly proportional to the oxygen permeation flux value, which leads to the development of an asymmetrical hollow fiber membrane design. As reported by Chi et al. (2017), the asymmetric pore configuration resulted in high surface area, good stability of the oxygen permeance, and

Production and hosting by Elsevier

H. Fansuri, Alfia Dewi Masyitoh, Silvana Dwi Nurherdiana et al.

*Journal of King Saud University – Engineering Sciences 35 (2023) 200–206*

mechanical strength. An asymmetric pore configuration means a thin and dense separation layer directly interconnected with a thick and porous layer (Chi et al., 2017; Iqbal et al., 2018a, 2018b).

The common technique to produce the inorganic or ceramic based-hollow fiber membranes is the extrusion-sintering method. In this technique, a mixture of raw materials consisting of ceramic powders, polymeric binders and additives (such as dispersants, plasticizers, and pore formers) is extruded using a spinneret to form hollow fiber membrane precursors by phase inversion process, followed by a high-temperature sintering process (Hussain et al., 2006). The membrane performance is strongly affected by its morphology and microstructure such as grain size and shape, porosity, pore size, and pore size distribution. Nevertheless, the membrane morphology can be modified by applying various compositions of the dope solution or the spinning parameters (Tan and Li, 2011). Some additives, such as polyvinyl pyrrolidone (PVP) (Song et al., 2017; Tan et al., 2011) and polyethylene glycol (PEG) or Arlacel P135 (Chi et al., 2017; Mohamed et al., 2016) have been used to modify the membrane morphology. Chakrabarty et al. (2008) also reported the molecular weight (MW) of PEG affected the morphology of the resulting flat polysulfone (PSf) membrane where the membrane porosity increased with the increase of PEG molecular weight due to increasing hydrophilicity of PEG. The higher the molecular weight of PEG, the more sponge-like pores were formed.

Studies related to the fabrication of membranes with PEG as an additive showed that PEG produces porous structures (Iqbal et al., 2018a, 2018b). However, the effect of PEG molecular weight on membrane morphology or pores towards the oxygen permeability has not been widely studied. This study investigate a series of LSCF 7328 (La$_{0.7}$Sr$_{0.3}$Co$_{0.2}$Fe$_{0.8}$O$_{3-\delta}$) hollow fiber membranes for oxygen separation which were prepared by various molecular weight PEG additive as pore forming agent.

## 2. Experimental

### 2.1. Materials

Powders of La$_2$O$_3$ (99,9%; Aldrich), SrCO$_3$ (99,9%; Aldrich), Co$_3$O$_4$ (Aldrich) and Fe$_2$O$_3$ (97%; Merck) were used as raw material to synthesize La$_{0.7}$Sr$_{0.3}$Co$_{0.2}$Fe$_{0.8}$O$_{3-\delta}$ (LSCF 7328) powder through a solid-state method as described in Fansuri et al. (2017). Polyethersulfone (PESf) (Radel A300, Ameco Performance, USA) and *N*-methyl-2-pyrollidone (NMP) (Merck) were used as polymer binder and solvent, respectively. Polyethylene glycol (PEG) (Merck) (MW = 2000, 3400 and 6000 Da) were used as an additive due to its ability to control the membrane morphology. The hollow fiber membranes were fabricated by phase-inversion method using tap water for both external coagulant and bore liquid. N$_2$ (UHP) was used to test the gas tightness property of the membranes while He (UHP) and compressed air were used as sweep gas and feed gas during the measurement of oxygen permeability.

### 2.2. Fabrication and characterization of the hollow fiber membranes

A highly asymmetrical structure of a single-layer hollow fiber membrane was fabricated by extrusion followed by sintering method. The method was adapted from Nurherdiana et al. (2019) where the spinning condition and dope composition were detailed in Table 1. The NMP solvent was poured into a ball mill jar, followed by the gradual addition of the synthesized LSCF 7328 powder and PEG with different molecular weight i.e. 2000, 3400 and 6000 Da. The mixture was then milled using a planetary ball mill (NQM-4, Yangzhou Nouya Machinery) at room temperature and 183 rpm for 24 h. PESf was then added to the milled suspension

**Table 1**
Spinning condition for fabrication of LSCF 7328 hollow fiber membranes.

| | | | |
|---|---|---|---|
| | LSCF 7328 57 wt% | Flow rate of bore liquid | 10 mL·min$^{-1}$ |
| Dope composition | PESf 6 wt% NMP 34 wt%t PEG 3 wt% | Extrusion rate Air gap Sintering temperature | 8 mL·min$^{-1}$ 10 cm 1250 °C |
| External coagulant Bore liquid (internal coagulant) | Water Tap water | Sintering time | 5 h |

before being milled again for 48 h to obtain a stable and homogeneous dope suspension (Chi et al., 2017; Mohamed et al., 2016). The viscosity of dope suspension was measured by a viscometer (DV-I Prime Viscometer, Brookfield Engineering, Middleboro) before being extruded into a hollow fiber.

The extrusion of the dope suspension was processed using the orifice-spinneret equipped with a syringe pump (Harvard Apparatus, Holliston, MA). The nascent membrane was immersed overnight in a coagulant bath, dried and straightened at ambient temperature. The sintering process was executed in a tubular furnace, started at room temperature and gradually increased to 400 °C at a heating rate of 5 °C·min$^{-1}$ and maintained for 2 h. Next, the temperature was increased again to 1250 °C at a heating rate of 10 °C·min$^{-1}$ and maintained for 5 h to sinter the membrane by allowing a fusion process and interconnection bonding among LSCF particles (Tan et al., 2001).

The hollow fiber membrane was then characterized by scanning electron microscopy (SEM, Hitachi TM-3000, Tokyo, Japan) to investigate the morphology of both cross-section and outer surface. Mercury porosimeter (Micromeritics V 9600) was applied to characterize the membrane porosity, whereas the mechanical strength was examined using a three point bending-test method (Instron Model 3342 Norwood). The hollow fiber membrane (6–9 cm in length) was placed on the centre of jigs then the crosshead was lowered at speed 0.1 N·min$^{-1}$ against the membrane. The maximum load of the membrane was recorded and calculated using Eq. 1 to find out the bending strength value. Furthermore, the surface tightness of the membrane was also investigated by gas tightness test method as described by Nurherdiana et al. (2019). The membrane sample (2–3 cm in length) was glued in a stainless steel adaptor using epoxy resin and assembled in a vessel. During the tightness test, N$_2$ was flown in a certain pressure while the changing pressure of N$_2$ gas was recorded and calculated using Eqs. (2) and (3) to determine the permeation value. The equations are based on (Mohamed et al., 2016).

$$B = \frac{8NLD_0}{\pi\left(D_o^4 - D_i^4\right)} \quad (1)$$

$$P = \frac{V}{RT \cdot A_t t}\ln\left(\frac{p_0 - p_a}{p_t - p_a}\right) \quad (2)$$

$$A_t = \frac{[\pi L(D_o - D_i)]}{\ln\frac{D_o}{D_i}} \quad (3)$$

where $A_t$ is defined as effective membrane area which determined by Eq. (3); B = bending strength of the hollow fiber membrane (MPa); N = maximum load of the sample (N); L = sample length (m); $D_o$ = outer diameter of the sample (m); $D_i$ = inner diameter of the sample (m); P = N$_2$ permeation of the membrane (mol·m$^{-2}$·s$^{-1}$·Pa$^{-1}$); V = permeation cell volume (m$^3$); R = gas constant (8.314 J·mol$^{-1}$·K$^{-1}$); T = temperature during the test (K); $p_0$ = initial

H. Fansuri, Alfia Dewi Masyitoh, Silvana Dwi Nurherdiana et al.

*Journal of King Saud University – Engineering Sciences 35 (2023) 200–206*

pressure (Pa); $p_t$ = final pressure (Pa) and $p_a$ = atmospheric pressure (Pa).

### 2.3. Oxygen permeation measurements

Oxygen permeation flux was measured using a gas chromatography (Buck Scientific GC Model 910) at atmospheric pressure (1 atm). The sintered hollow fiber membrane was glued in a quartz tube using ceramic glue. Another quartz tube was placed in an alumina tube which contributed to He sweep gas pipeline. The sweep gas flow rate was adjusted at 150 mL·min$^{-1}$ by a mass flow controller (MFC, Omega FMA5400/5500) then compressed air was flown on the top of the membrane as a feed gas at 30 mL·min$^{-1}$. All the reactor tubes were placed in the centre of the tubular furnace to maximize the heating process.

The measurement was executed at 750 °C with 30 min holding time and the permeation flux was calculated by Eq. (4) where $J_{O_2}$ is oxygen permeation flux (mol·s$^{-1}$·cm$^{-2}$), F is sweep gas (He) flow rate (mL·min$^{-1}$), $C_{O_2}$ is oxygen concentration in the permeate which was successfully separated from the air (mol·mL$^{-1}$) and $A_t$ is effective surface area of the membrane (cm$^2$) which calculated from Eq. (3).

$$J_{O_2} = \frac{F \times C_{O_2}}{At} \tag{4}$$

## 3. Result and discussion

### 3.1. Fabrication and characterization of LSCF hollow fiber membrane

#### 3.1.1. Viscosity of dope suspension using different molecular weight of PEG

The preparation of dope suspension was started by LSCF 7328 sieving (400 mesh) to obtain uniform and small size powder to produce a high membrane tightness. Smaller powder size produced tighter membrane surface (Chi et al., 2017). During dope preparation, LSCF 7328 powder was added into NMP solvent gradually to avoid agglomeration then stirred overnight and then 3 wt% of PEG was added gradually into the mixture. In order to compare the viscosity and other characteristics, a hollow fiber membrane without PEG addition was also fabricated as control. It was found that the larger molecular weight of PEG additive increase dope viscosity as shown in Table 2.

The result is similar to the report by Idris et al. (2007) who used PEG 200, 400 and 600 Da to fabricate polyethersulfone hollow fiber membrane. The authors reported that the dope viscosity increased as increase of PEG molecular weight. The larger molecular weight of PEG revealed higher dope viscosity which related to its long polymeric chain and bulk molecular size (Nurherdiana et al., 2019).

#### 3.1.2. Morphology of hollow fiber membrane

The morphology of membrane precursors before being sintered are shown in Fig. 1. The images show asymmetric structure that contains a dense layer on top of the finger-like porous layer. The size of the outer and inner diameter of each membrane was 1.97 and 1.45 mm for HF; 2.30 and 1.65 mm for HF-P1; 2.09 and 1.50 mm for HF-P2; and 2.12 and 1.16 mm for HF-P3, respectively.

**Table 2**
Viscosity of dope suspension in various molecular weight of PEG.

| Hollow fiber membrane | | Viscosity (cP) |
|---|---|---|
| HF | LSCF (with no PEG) | 2990.0 |
| HF-P1 | LSCF-PEG 2000 | 3821.7 |
| HF-P2 | LSCF-PEG 3400 | 4430.0 |
| HF-P3 | LSCF-PEG 6000 | 7710.0 |

The asymmetric structure of the pore configuration had been obtained from the impact of solidification process where solvent (NMP) molecule was replaced by water as a coagulant via a diffusion mechanism. The NMP solvent was diffused out of the membrane, while the water molecule was diffused in that makes the membrane harden and denser. The exchange mechanism of solvent and non-solvent molecule resulted in increasing polymer concentration and was followed by the solidification process of the membrane (Ilham et al., 2018). This phenomenon is well-known as a phase-inversion mechanism. The nascent membrane was then dried and straightened at ambient temperature to produce membrane precursor

In addition, PEG, as an additive, control the exchange rate between solvent and non solvent to form pores and macro-voids. Fig. 1 showed that the addition of PEG with a molecular weight of 2000, 3400 and 6000 Da produced membrane precursors with a finger-like pore structure. It is also confirmed that the PEG addition into the dope suspension reduces the diffusion rate of solvents (NMP) and non-solvents (water) exchange. PEG has a high solubility in water which easily diffuses from the membranes into the water and leaves traces to form finger-like pore which is consistent with the report by Saljoughi et al. (2010).

After sintering at 1250 °C, all membranes were shrank as evidenced by the reduced size of both the outer and inner diameters. After sintering, the size of outer and inner diameter, respectively, of HF membrane were 1.92 and 1.38 mm; HF-P1 were 1.60 and 1.14 mm; HF-P2 were 1.43 and 0.963 mm; while HF-P3 were 1.78 and 1.15 mm. The difference of membrane diameter before and after sintering and the shrinkage value for each membrane are detailed in Table 3. The shrinkage ratio is defined as ratio of the outer diameter (o.d) of the sintered hollow fiber to the outer diameter (o.d) of the hollow fiber precursor before sintering (Tan et al., 2001). The shrinkage was caused by the loss of polymeric molecules (binder) and additives which was burnt off in air at temperature above 300 °C (Athayde et al., 2015), followed by sintering of LSCF particles to form denser membranes at 1250 °C. However, in general, there were no significant changes in membrane morphology before and after sintering. The main structure of the membrane was still be maintained but the pore structure of the sintered membrane becomes clearer than that of the membrane precursor which indicates that sintering did not change the overall structure (Tan et al., 2011) although according to Tan et al. (2005a) the number and size of the membranes' pores tend to decrease.

The formation of dense morphology was also observed on the surface of the hollow fiber membranes. The SEM images of the outer surface of the membranes before and after sintering are presented in Fig. 2 where the morphology differences of outer surface of precursor and sintered membrane are observed. The outer surface of membrane precursor show that the LSCF particles are evenly spread or well-dispersed. Despite its tenuous distribution, the particles are connected to each other by polymer binders. On the other hand, the outer surface of the sintered membrane shows that the polymer binder has disappeared and the LSCF particles are connected to each other to form larger particles with visible grain boundaries. The results are similar to the report by Tan et al. (2005a), Tan et al. (2005b) who produced a compact hollow fiber membrane after sintering at 1280 °C. The SEM images also show that the use of the higher molecular weight of PEG produced more cavities. The cavities might be the enlargement of finger-like pores (Nurherdiana et al., 2019).

In general, there were no significant changes in membrane morphology before and after sintering. After sintering, the HF-P1 membrane formed a grain size that was larger than the other membranes. When the sintering process was carried out, the removal of polymer components in the membrane precursors causes the LSCF particles to be interconnected and formed larger
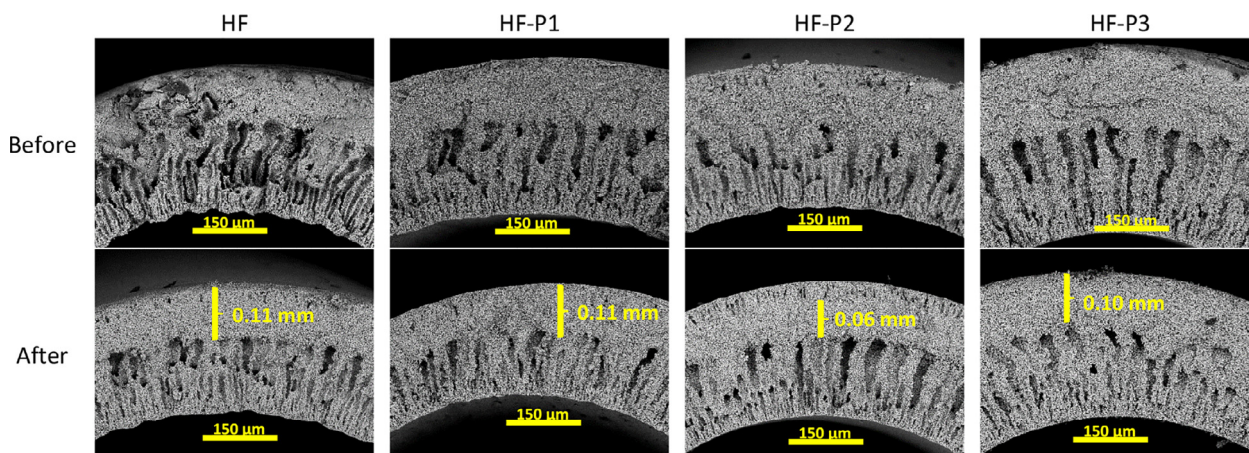
H. Fansuri, Alfia Dewi Masyitoh, Silvana Dwi Nurherdiana et al.

Journal of King Saud University – Engineering Sciences 35 (2023) 200–206

**Fig. 1.** SEM images of membrane before and after sintering at 1250 °C.

**Table 3**
Outer diameter (o.d), inner diameter (i.d) and shrinkage value of hollow fiber membrane with different molecular weight of PEG.

| Membrane | Before sintering | | After sintering | | Shrinkage (%) |
|---|---|---|---|---|---|
| | o.d (mm) | i.d (mm) | o.d (mm) | i.d (mm) | |
| HF | 1.97 | 1.45 | 1.92 | 1.38 | 2.54 |
| HF-P1 | 2.30 | 1.65 | 1.60 | 1.14 | 30.43 |
| HF-P2 | 2.09 | 1.50 | 1.43 | 0.96 | 31.58 |
| HF-P3 | 2.12 | 1.16 | 1.78 | 1.15 | 16.04 |
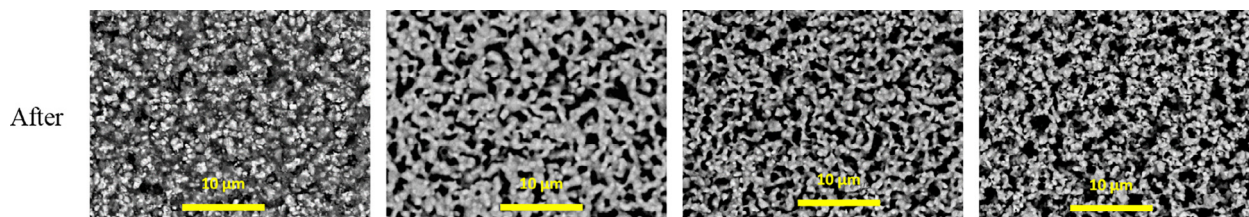


**Fig. 2.** Close-up SEM images of surface membrane morphology before and after sintering.

grains. Thus, in the HF-P1 membrane large particle granules and large sponge-like pores were formed. Meanwhile, in the HF-P2 and HF-P3 the size of granules and pores is smaller than HF-P1. However, the number of pores in HF-P2 and HF-P3 is greater and evenly distributed.

Additionally, the porous structures formed on the membrane surface indicated that the sintering temperature was not sufficient to form a dense membrane. According to Tan et al. (2005a), Tan et al. (2005b), the formation of dense structure on LSCF based hollow fiber membrane requires a sintering temperature of 1280 °C and a holding time of 4 h. At 1280 °C the LSCF particles in the membrane melt and connected to form a perfectly compact structure. Sintering of hollow fiber at high temperatures leads to an increase in the membrane density, which can be confirmed by the gas tightness test result. Tan et al. (2001) explained that sintering temperature is a very influential factor in membrane density and mechanical strength.

### 3.1.3. Gas tightness of hollow fiber membrane

In this study, the separation of oxygen from air is based on the ability of the lattice structure in perovskite with reactions described in detailed (Nurherdiana et al., 2019; Wang et al., 2002). Therefore, it requires dense outer layer to prevent any leakage which may causes undesirable mixing of uncontrollable supply of oxygen and methane into the reaction system.

Gas tightness test was mostly used to measure the density of the particles of the membrane, especially on the outer layer membranes. Fig. 3 shows the $N_2$ tightness test result of the present work. The molecular weight of PEG does affect the density of hol-
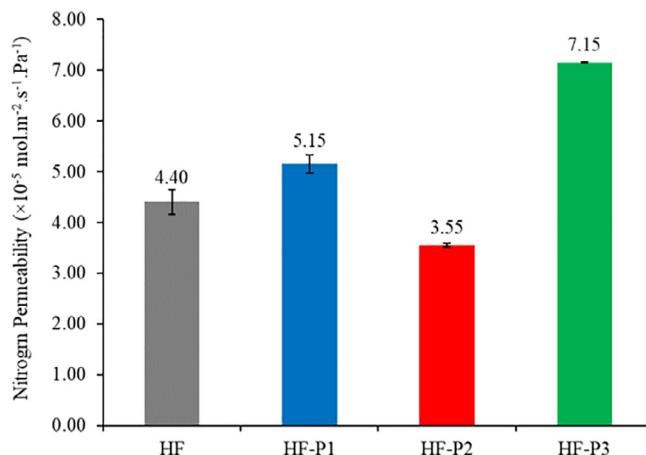


**Fig. 3.** $N_2$ permeability of hollow fiber membranes with various molecular weight of PEG.

H. Fansuri, Alfia Dewi Masyitoh, Silvana Dwi Nurherdiana et al.

*Journal of King Saud University – Engineering Sciences 35 (2023) 200–206*

low fiber membranes. Although it seems that the effect is fluctuating, in overall, the density of membranes decreases as the increase of the molecular weight of PEG additive.

The tightest hollow fiber membrane is achieved by HF-P2 with $N_2$ permeability of $3.55 \times 10^{-5}$ mol·m$^{-2}$·s$^{-1}$·Pa$^{-1}$, which is lower than the previous work of Sajidah et al., (2018) and Mohamed et al. (2016) which shows that the hollow fiber membrane in this study have a better density. In addition, HF-P2 also has a dense layer in the middle of hollow fiber membrane that makes the gas diffusion pathway was smaller which lead to lower $N_2$ permeability.

Table 4 presents the comparison of $N_2$ permeability in this work with several previous studies.

It can be seen that the HF-P2 membrane showed a very low density among the others. The difference can be explained from the sintering temperature which was 1250 °C (with holding time of 5 h). A hollow fiber membrane can be assumed as a gas-tight membrane if the measured $N_2$ permeability is lower than $10^{-10}$ mol·m$^{-2}$·s$^{-1}$·Pa$^{-1}$ or around $10^{-11}$ mol·m$^{-2}$·s$^{-1}$·Pa$^{-1}$ (Liu et al., 2001; Tan et al., 2005b). For this reason, it can be concluded that the sintering temperature of 1250 °C is inadequate to form a high density perovskite-based hollow fiber membrane.

### 3.1.4. Porosity and pore size distribution of hollow fiber membrane

As a porous ceramic membrane, the hollow fiber must provide sufficient pores for mass transport and have a small pore size distribution for high selectivity. The porosity of the membranes and average pore diameter are shown in Fig. 4. The porosity tends to decrease with an increase molecular weight of PEG additive. HF-P1 showed the highest porosity among the others at 5.74%. HF-P2 produced a porosity of 5.46%, while the lowest porosity was shown by HF-P3 which is 5.34%. The average pore diameter of the membranes in Fig. 4 also shows the same tendency with the membrane porosity. The average pore diameters of HF-P1, HF-P2, and HF-P3 ($\times 10^3$ nm) are 85.29; 4.89; and 1.88, respectively. A significant difference can be observed in the figure where the highest molecular weight of PEG produced the lowest average pore diameter.

The percentage of porosity and average pore diameter in Fig. 4 are overall measurement results for each pore contained in the hollow fiber membranes. Therefore, a comparison of mercury intrusion data of each hollow fiber is needed to determine the distribution of its pore size. Fig. 5 presents the pore size distribution for all PEG variations, where the smallest to the largest pores exist in the membranes.

Fig. 5 shows that each variation of hollow fiber membranes consisted of two main types of pores, i.e., regions with sponge-like structure and the entrance of the finger-like structure. HF-P1 and

**Table 4**
$N_2$ permeability of ceramic-based hollow fiber membranes with various sintering temperature (taken at room temperature and 1 atm).

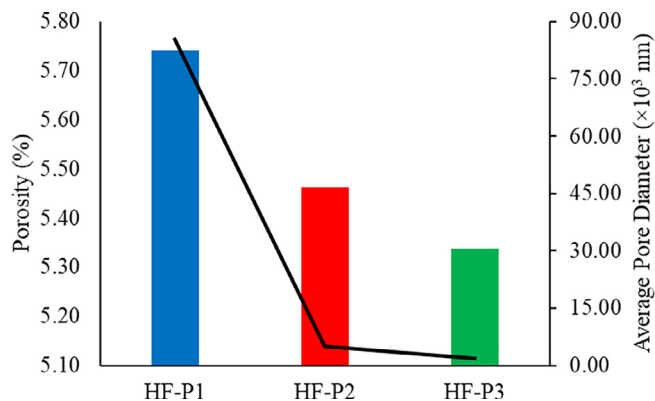| Membrane | $N_2$ permeability (mol·m$^{-2}$·s$^{-1}$·Pa$^{-1}$) | Sintering temperature (°C) | Reference |
|---|---|---|---|
| HF | $4.40 \times 10^{-5}$ | 1250 | This work |
| HF-P1 | $5.15 \times 10^{-5}$ | 1250 | |
| HF-P2 | $3.55 \times 10^{-5}$ | 1250 | |
| HF-P3 | $7.15 \times 10^{-5}$ | 1250 | |
| LSCF-YSZ/ NiO-YSZ | $1.364 \times 10^{-5}$ | 1300 | Sajidah et al. (2018) |
| LSCF | $2.82 \times 10^{-10}$ | 1280 | Tan et al. (2005b) |
| Non-porous | $10.6 \times 10^{-7}$ | 1400 | Wei and Li |
| YSZ | $2.0 \times 10^{-10}$ | 1500 | (2008) |
| SCYb/PESf | $<3.0 \times 10^{-10}$ | 1500 | Liu et al. |
| | $6.45 \times 10^{-10}$ | 1550 | (2001) |



**Fig. 4.** Porosity and average pore diameter of hollow fiber membranes.
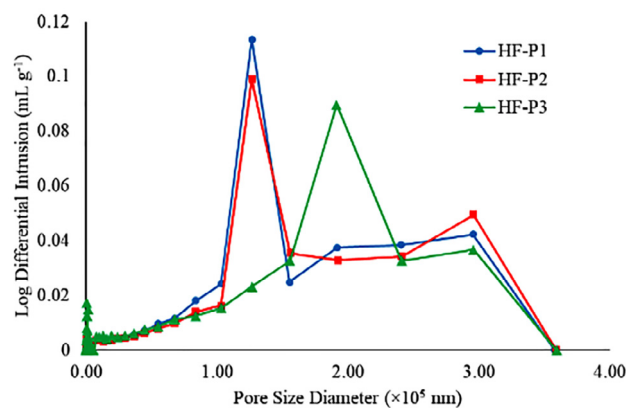


**Fig. 5.** Pore size distribution of hollow fiber membranes with various molecular weight of PEG.

HF-P2 hollow fibers showed a sponge-like pore size distribution at a peak of about $1.27 \times 10^5$ nm. The distribution shifted to peak $1.91 \times 10^5$ nm, approximately, indicated an increasing pore size diameter. The finger-like pore region of the three membrane types is shown at a peak of about $1.91 \times 10^5$ nm. The decrease in peak intensity implied increasing dope viscosity (Othman et al., 2010) due to the increasing molecular weight of PEG, as previously explained.

### 3.1.5. Mechanical properties of hollow fiber membrane

The mechanical strength of the membrane was tested by a three-point-bending method and the results are shown in Fig. 6.

Tan et al. (2011) reported that membranes with a finger-like pore structure have better mechanical strength than membranes with a sponge-like pore structure. In addition, Mohamed et al. (2016) reported that the use of pure water as a bore liquid can affect the mechanical strength of hollow fiber membranes.

Fig. 6 shows that the HF-P1 hollow fiber membrane has the highest mechanical strength (11.51 MPa) as compared to the remaining membranes. Comparatively, hollow fiber membrane without PEG addition has the lowest mechanical strength (3.48 MPa). The trends in mechanical strength is consistent with membrane morphology as shown in Fig. 2. Membranes with PEG additive, were sintered better than membrane with no PEG. The PEG improves the density of green membrane (un-sintered membrane) which led to more intensive sintering of LSCF particles (Zare et al., 2019), resulting stronger membranes than membrane with no PEG additive. In addition, the decrease in the mechanical
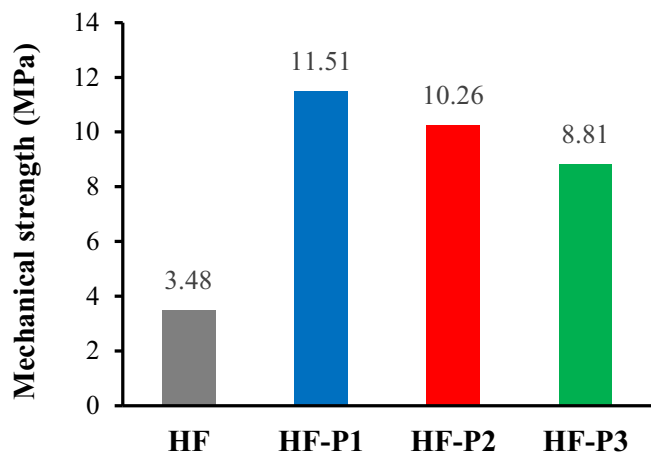
H. Fansuri, Alfia Dewi Masyitoh, Silvana Dwi Nurherdiana et al.

Journal of King Saud University – Engineering Sciences 35 (2023) 200–206



**Fig. 6.** The mechanical strength of membrane with various molecular weight of PEG.

strength of membranes with increasing PEG molecular weight might be caused by the formation of larger and finger-like pores in the membrane. Similar results were also reported by Aminudin et al., (2013).

*3.2. Oxygen permeability*

The oxygen permeation test was performed using compressed air as feed gas as referred to Sajidah et al. (2018). The results for all membranes are shown in Fig. 7. It can be seen that HF-P2 achieved the highest oxygen permeation flux of $6.07 \times 10^{-8}$ mol·cm$^{-2}$·s$^{-1}$ as compared to the remaining membranes. The oxygen permeation of HF-P3 membrane is $5.06 \times 10^{-8}$ mol·cm$^{-2}$·s$^{-1}$, while HF-P1 and HF is only slightly different ($4.71 \times 10^{-8}$ mol·cm$^{-2}$·s$^{-1}$ and $4.72 \times 10^{-8}$ mol·cm$^{-2}$·s$^{-1}$, respectively). It indicates that the different thickness of the sponge-like pore contributes to different oxygen permeation values as detailed in Table 5.

The addition of PEG into the dope suspension can improve the membrane performance to deliver oxygen, as a consequence of the additive diffusion which enlarges the membrane pore and reduces the dense layer. From Table 5, it was found that that the thickness of the dense layer affects the oxygen permeation of the
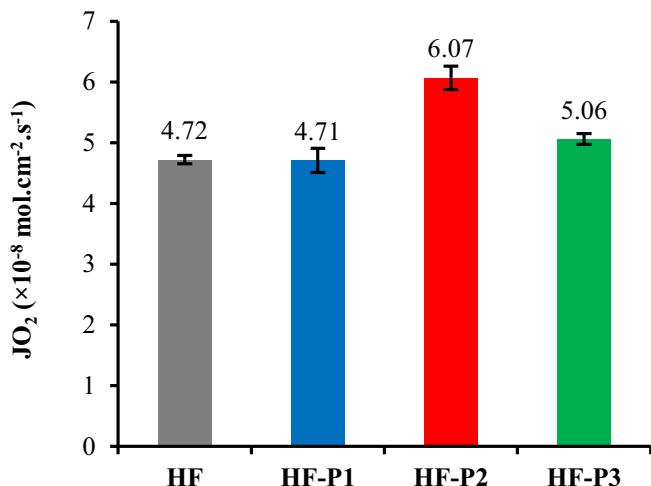
**Table 5**
Dense layer thickness of membranes in various molecular weight of PEG.

| Membrane | $J_{O_2}$ flux ($\times 10^{-8}$ mol·cm$^{-2}$·s$^{-1}$) | Dense layer thickness (mm) | Standard deviation of $J_{O_2}$ |
|---|---|---|---|
| HF | 4.72 | 0.11 | 0.011 |
| HF-P1 | 4.71 | 0.11 | 0.010 |
| HF-P2 | 6.07 | 0.06 | 0.009 |
| HF-P3 | 5.06 | 0.10 | 0.005 |

membrane. HF-P2 has the lowest thickness so that the oxygen flux produced is the highest among the others. The oxygen permeation of HF-P3 is lower than HF-P2 because it has a thicker dense layer. Meanwhile, the oxygen permeation of HF-P1 is closely the same as HF, due to the similar dense layer thickness.

Oxygen is transported from one side of membrane to the other through oxygen vacancies in the membrane lattice. Pores in the membranes break the continuity of membrane lattice that makes the energy requirement for oxygen transport increase. The oxygen must jump over the empty space formed by the pore so that the oxygen can occupy oxygen vacancies on the other side of the pore wall. Therefore, as the membrane porosity decrease due to increasing PEG molecular weight, the oxygen flux of the membrane increases.

The obtained oxygen flux result in this study is higher than the value as reported by Sajidah et al. (2018). It could be caused by different membrane thicknesses and designs. The single-layer hollow fiber in this study was only fabricated from LSCF 7328 without any additional material, thus the oxygen transport could be maximized through the oxygen vacancy mechanism on the perovskite lattice. Other factors that might also affect the oxygen flux are not studied in this article.

**4. Conclusion**

In this study, the LSCF hollow fiber membrane with the addition of the various molecular weight of PEG was investigated to optimize the type of PEG on the membrane properties for oxygen permeation applications. The PEG addition exhibited asymmetrical pore configuration which sponge-like integrated the finger-like pore. Hollow fiber membrane density was also tested by measuring $N_2$ permeability which showed that hollow fiber with additive PEG 3400 Da revealed the densest membrane with the lowest $N_2$ permeability of $3.55 \times 10^{-5}$ mol·m$^{-2}$·s$^{-1}$·Pa$^{-1}$. Overall porosity of hollow fiber membranes decreases with the increase of molecular weight of PEG. The highest mechanical strength of the membrane was produced by hollow fibers with the PEG 2000 Da additive. The increase in the molecular weight of PEG decreases the mechanical strength of the LSCF membrane, which affected by the irregular pore configuration. The addition of PEG additives with various molecular weights results in different dense layer thicknesses so that it affected the oxygen permeation flux. The highest oxygen permeation flux was achieved using a hollow fiber membrane with PEG 3400 Da, with a flux value of $6.07 \times 10^8$ mol·cm$^{-2}$·s$^{-1}$ which supported by the thinnest dense layer of 0.06 mm.

**Declaration of Competing Interest**

The authors declare that they have no known competing financial interests or personal relationships that could have appeared to influence the work reported in this paper.

**Fig. 7.** Oxygen permeation flux of the hollow fiber membranes with various molecular weight of PEG.

H. Fansuri, Alfia Dewi Masyitoh, Silvana Dwi Nurherdiana et al.

Journal of King Saud University – Engineering Sciences 35 (2023) 200–206

# References

Akulinin, E., Golubyatnikov, O., Dvoretsky, D., Dvoretsky, S., 2020. Optimization and analysis of pressure swing adsorption process for oxygen production from air under uncertainty. Chem. Ind. Chem. Eng. Q. 26 (1), 89–104. https://doi.org/10.2298/CICEQ190414028A.

Aminudin, N.N., Basri, H., Harun, Z., Yunos, M.Z., Sean, G.P., 2013. Comparative study on effect of PEG and PVP as additives on polysulfone (PSF) membrane structure and performance. J. Teknol. (Sci. Eng.) 65, 47–51. https://doi.org/10.11113/jt.v65.2327.

Athayde, D.D., Souza, D.F., Silva, A.M.A., Vasconcelos, D., Nunes, E.H.M., Diniz da Costa, J.C., Vasconcelos, W.L., 2015. Review of perovskite ceramic synthesis and membrane preparation methods. Ceram. Int. 42, 6555–6571. https://doi.org/10.1016/j.ceramint.2016.01.130.

Chakrabarty, B., Ghoshal, A.K., Purkait, M.K., 2008. Effect of molecular weight of PEG on membrane morphology and transport properties. J. Memb. Sci. 309 (1–2), 209–221. https://doi.org/10.1016/j.memsci.2007.10.027.

Chi, Y., Li, T., Wang, B., Wu, Z., Li, K., 2017. Morphology, performance and stability of multi-bore capillary $La_{0.6}Sr_{0.4}Co_{0.2}Fe_{0.8}O_{3-\delta}$ oxygen transport membranes. J. Memb. Sci. 529, 224–233. https://doi.org/10.1016/j.memsci.2017.02.010.

Ettouney, H.M., Fakeeha, A.H., Helal, A., Hughes, R., 1995. Factors affecting enrichment of natural gas by polymeric membranes. J. King Saud Univ. – Eng. Sci. 7, 35–60. https://doi.org/10.1016/S1018-3639(18)31050-X.

Fansuri, H., Syafi'i, M.I., Romdoni, S., Masyitoh, A.D., Utomo, W.P., Prasetyoko, D., Widiastuti, N., Murwani, I.K., Subaer, 2017. Preparation of dense $BaxSr1-xCo0.8Fe0.2O3$ membranes: effect of Ba2+ substituents and sintering method to the density, hardness and thermal expansion coefficient of the membranes. Adv. Mater. Lett. 8, 799–806. https://doi.org/https://doi.org/c

Hussain, A.A., Abashar, M.E.E., Al-Mutaz, I.S., 2006. Effect of ion sizes on separation characteristics of nanofiltration membrane systems. J. King Saud Univ. – Eng. Sci. 19 (1), 1–18. https://doi.org/10.1016/S1018-3639(18)30844-4.

Ilham, A.M., Khoiroh, N., Jovita, S., Iqbal, R.M., Harmelia, L., Nurherdiana, S.D., Utomo, W.P., Fansuri, H., 2018. Morphological and physical study of $La_{0.7}Sr_{0.3}Co_{0.2}Fe_{0.8}O_{3-\delta}$ (LSCF 7328) flat membranes modified by polyethylene glycol (PEG). J. Appl. Membr. Sci. Technol. 22, 119–130. https://doi.org/10.11113/amst.v22n2.131.

Iqbal, R.M., Nurherdiana, S D, Sahasrikirana, M.S., Harmelia, L., Utomo, W.P., Setyaningsih, E.P., Fansuri, H., 2018. The compatibility of NiO, CeO2 and NiO-CeO2 as coating on La0.6Sr0.4Co0.2Fe0.8O3-δ, La0.7Sr0.3Co0.2Fe0.8O3−δ and La0.7Sr0.3Mn0.3O3-δ ceramic membranes and their mechanical properties the compatibility of NiO, CeO2 and NiO-CeO2 as a coating. In: IOP Conference Series: Materials Science and Engineering, p. 012032. https://doi.org/10.1088/1757-899X/367/1/012032

Iqbal, R.M., Nurherdiana, S.D., Hartanto, D., Othman, M.H.D., Fansuri, H., 2018. Morphological control of La0.7Sr0.3Co0.2Fe0.8O3−δ and La0.7Sr0.3MnO3−δ catalytic membrane using PEG-H2O additive. In: IOP Conference Series: Materials Science and Engineering, p. 012008. https://doi.org/10.1088/1757-899X/348/1/012008

Liu, S., Tan, X., Li, K., Hughes, R., 2001. Preparation and characterisation of $SrCe_{0.95}Yb_{0.05}O_{2.975}$ hollow fibre membranes. J. Memb. Sci. 193 (2), 249–260. https://doi.org/10.1016/S0376-7388(01)00518-X.

Mohamed, M.H., Othman, M.H.D., Mutalib, A.M., Rahman, M., Jaafar, J., Ismail, A.F., Dzahir, M.I.H.M., 2016. Structural control of NiO-YSZ/LSCF-YSZ dual-layer hollow fiber membrane for potential syngas production. Int. J. Appl. Ceram. Technol. 13, 799–809. https://doi.org/10.1111/ijac.12561.

Murali, R.S., Sankarshana, T., Sridhar, S., 2013. Air separation by polymer-based membrane technology. Sep. Purif. Rev. 42 (2), 130–186. https://doi.org/10.1080/15422119.2012.686000.

Nurherdiana, S.D., Utomo, W.P., Sajidah, H.B.N., Jamil, S.M., Othman, M.H.D., Fansuri, H., 2019. Comprehensive study of morphological modification of dual-layer hollow fiber membrane. Arab. J. Sci. Eng. 44 (12), 10041–10055. https://doi.org/10.1007/s13369-019-04057-5.

Othman, M.H.D., Droushiotis, N., Wu, Z., Kanawka, K., Kelsall, G., Li, K., 2010. Electrolyte thickness control and its effect on electrolyte/anode dual-layer hollow fibres for micro-tubular solid oxide fuel cells. J. Memb. Sci. 365 (1–2), 382–388. https://doi.org/10.1016/j.memsci.2010.09.036.

Rossetti, I., Compagnoni, M., Finocchio, E., Ramis, G., Di Michele, A., Zucchini, A., Dzwigaj, S., 2016. Syngas production via steam reforming of bioethanol over Ni-BEA catalysts: a BTL strategy. Int. J. Hydrogen Energy 41 (38), 16878–16889.

Sajidah, H.B.N., Nurherdiana, S.D., Utomo, W.P., Iqbal, R.M., Hartanto, D., Othman, M. H.D., 2018. Preparation and characterization of dual-layer hollow fibre catalyst membrane for oxygen transport preparation and characterization of dual-layer hollow fibre catalyst membrane for oxygen transport. In: AIP Conference Proceedings, pp. 020090-1–020090-8. https://doi.org/https://doi.org/10.1063/1.5082495

Saljoughi, E., Amirilargani, M., Mohammadi, T., 2010. Effect of PEG additive and coagulation bath temperature on the morphology, permeability and thermal/chemical stability of asymmetric CA membranes. Desalination 262, 72–78. https://doi.org/10.1016/j.desal.2010.05.046.

Song, Z., Zhang, Z., Zhang, G., Liu, Z., Zhu, J., Jin, W., 2017. Effects of polymer binders on separation performance of the perovskite-type 4-bore hollow fiber membranes. Sep. Purif. Technol. 187, 294–302. https://doi.org/10.1016/j.seppur.2017.06.063.

Tan, X., Li, K., 2011. Inorganic hollow fibre membranes in catalytic processing. Curr. Opin. Chem. Eng. 1, 69–76. https://doi.org/10.1016/j.coche.2011.08.004.

Tan, X., Liu, N., Meng, B., Liu, S., 2011. Morphology control of the perovskite hollow fibre membranes for oxygen separation using different bore fluids. J. Memb. Sci. 378, 308–318. https://doi.org/10.1016/j.memsci.2011.05.012.

Tan, X., Liu, S., Li, K., 2001. Preparation and characterization of inorganic hollow fiber membranes. J. Memb. Sci. 188 (1), 87–95. https://doi.org/10.1016/S0376-7388(01)00369-6.

Tan, X., Liu, Y., Li, K., 2005a. Preparation of LSCF ceramic hollow-fiber membranes for oxygen production by a phase-inversion/sintering technique. Ind. Eng. Chem. Res. 44 (1), 61–66. https://doi.org/10.1021/ie040179c.

Tan, X., Liu, Y., Li, K., 2005b. Mixed conducting ceramic hollow-fiber membranes for air separation. AIChE. J. 51 (7), 1991–2000. https://doi.org/10.1002/(ISSN)1547-590510.1002/aic.v51:710.1002/aic.10475.

Wang, H., Cong, Y., Yang, W., 2002. Oxygen permeation study in a tubular $Ba_{0.5}Sr_{0.5}Co_{0.8}Fe_{0.2}O_{3-\delta}$ oxygen permeable membrane. J. Memb. Sci. 210, 259–271. https://doi.org/10.1016/S0376-7388(02)00361-7.

Wei, C.C., Li, K., 2008. Yttria-stabilized zirconia (YSZ)-based hollow fiber solid oxide fuel cells. Ind. Eng. Chem. Res. 47 (5), 1506–1512. https://doi.org/10.1021/ie070960v.

Zare, M.H., Hajilary, N., Rezakazemi, M., 2019. Microstructural modifications of polyethylene glycol powder binder in the processing of sintered alpha alumina under different conditions of preparation. Mater. Sci. Energy Technol. 2 (1), 89–95. https://doi.org/10.1016/j.mset.2018.11.003.